J Mater Sci (2010) 45:4672–4681
DOI 10.1007/s10853-010-4462-z

ULTRAFINE GRAINED MATERIALS

EBSD characterization of an ECAP deformed Nb single crystal

Liang Zhu · Hugo R. Z. Sandim · Marc Seefeldt · Bert Verlinden

Received: 12 February 2010 / Accepted: 1 April 2010 / Published online: 15 April 2010

Abstract A niobium single crystal was subjected to equal channel angular pressing (ECAP) at room temperature after orienting the crystal such that [1 −1 −1] ‖ ND, [0 1 −1] ‖ ED, and [−2 −1 −1] ‖ TD. Electron backscatter diffraction (EBSD) was used to characterize the microstructures both on the transverse and the longitudinal sections of the deformed sample. After one pass of ECAP the single crystal exhibits a group of homogeneously distributed large misorientation sheets and a well formed cell structure in the matrix. The traces of the large misorientation sheets match very well with the most favorably oriented slip plane and one of the slip directions is macroscopically aligned with the simple shear plane. The lattice rotation during deformation was quantitatively estimated through comparison of the orientations parallel to three macroscopic axes before and after deformation. An effort has been made to link the microstructure with the initial crystal orientation. Collinear slip systems are believed to be activated during deformation. The full constraints Taylor model was used to simulate the orientation evolution during ECAP. The result matched only partially with the experimental observation.

L. Zhu (✉) · M. Seefeldt · B. Verlinden
Department of Metallurgy and Materials Engineering, Katholieke Universiteit Leuven, Kasteelpark Arenberg 44, 3001 Heverlee, Belgium
e-mail: liang.zhu@mtm.kuleuven.be

M. Seefeldt
e-mail: marc.seefeldt@mtm.kuleuven.be

B. Verlinden
e-mail: bert.verlinden@mtm.kuleuven.be

H. R. Z. Sandim
Department of Materials Engineering, University of Sao Paulo, P.O. Box 116, Lorena 12600-970, Brazil
e-mail: hsandim@demar.eel.usp.br

Introduction

Significant progress has been made recently in the analysis of the microstructural development during plastic deformation with small to medium strain [1–5]. The deformation-induced dislocation structures were widely studied for different deformation modes, mainly for tension, rolling, and channel die compression. Typical dislocation structures in FCC and BCC materials of medium to high stacking fault energy deformed to low and intermediate strains consist of two classes of dislocation boundaries: geometrically necessary boundaries (GNBs) and incidental dislocation boundaries (IDBs). The dependence of the dislocation structures on the grain orientation and slip systems have been reviewed and three types of dislocation structures have been established [6, 7]. One of them is a cell structure without GNBs. The other two are cell-block structures with cell-block boundaries (GNBs) aligned approximately parallel to the slip planes (within 10°) and deviated from the slip plane by more than 10°, respectively [6]. Slip systems are categorized into different classes and each slip class leads to a unique dislocation structure [7]. However, most of these microstructural studies were conducted on FCC materials. Much less is known on the microstructural evolution of BCC materials.

Equal channel angular pressing (ECAP) is one of the severe plastic deformation modes that have been developed during the past decades [8–10]. During ECAP, a lubricated billet is pressed through a rigid die consisting of two channels of the same cross-section, intersecting each other at an angle Φ. The aim is to impose extremely large strains

onto materials without generating a shape change and to produce ultrafine-grained materials. The underlying deformation mode is often approximated as simple shear on the intersecting plane [8], but the precise deformation mechanisms are not completely clear.

In this study, a niobium single crystal with a well chosen orientation was deformed by ECAP for only one pass, with a true strain of 1.15. Then, electron backscatter diffraction (EBSD) characterization was conducted on both the transverse and the longitudinal sections. The relationship between the initial crystal orientation and the alignment of the dislocation structures was established. The full constraints Taylor model was used to simulate the slip system activity during ECAP. The obtained result was compared with the experimental observations.

Experimental

Geometry of the specimen

The single crystal used in the current study was cut out from a high purity coarse-grained niobium ingot processed by electron beam melting. The contents of oxygen and nitrogen are 30 and 5 wt ppm, respectively [11]. The single crystal was machined into a cylindrical billet with a diameter of 11.9 mm and length of 60 mm. To understand the role of the initial crystallographic orientation on the substructure development during ECAP, the initial orientation was chosen as shown in Fig. 1a. This figure shows a schematic of the ECAP die and the initial orientation of the single crystal, i.e., [1 −1 −1] ∥ ND, [0 1 −1] ∥ ED, and [−2 −1 −1] ∥ TD. The corresponding pole figure (see Fig. 1b) shows the initial position of six {1 1 0} planes.

The ECAP procedure

The ECAP die used in this study has an abrupt angle Φ of 90° as shown in Fig. 1. The angle of curvature, ψ, denoting the outer arc of curvature where the two parts of the channel intersect, is 0°. The single crystal was pressed through the ECAP die for only one pass at room temperature with an extrusion rate of 10 mm/min. MoS_2 based grease was used to minimize the friction. The ECAP die has a circular cross-section with a diameter of 12.1 mm at the inlet and with a diameter of 11.7 mm at the outlet. The corresponding true strain (ε) per pass is 1.15 according to Eq. 1:

$$\varepsilon_{vM} = \frac{2N\cot(\varphi/2)}{\sqrt{3}} \quad (1)$$

where N is the number of passes [12].

Sample preparation

After ECAP, both ends of the ECAPed samples were removed. The middle part was used to prepare samples for microstructural examination of the ND–TD section (transverse) and the ND–ED section (longitudinal). A slow cutting diamond saw was used to reduce the depth of the damaged layer caused by mechanical machining. Microstructural characterization was performed using EBSD on a scanning electron microscope (FEI-XL30) operating at 20 kV with a tungsten filament. To obtain the high quality of the sample surface required for good EBSD scans, the samples were first ground with grit SiC up to 4000 mesh, followed by attack-polishing with a 260 mL commercial colloidal silica suspension +40 mL hydrogen peroxide (H_2O_2). Afterwards, electropolishing was performed using a solution consisting of 30 mL HF + 40 mL H_2SO_4 + 130 mL lactic acid at 20 V with a current of 250 mA at −5 °C for 2 min.

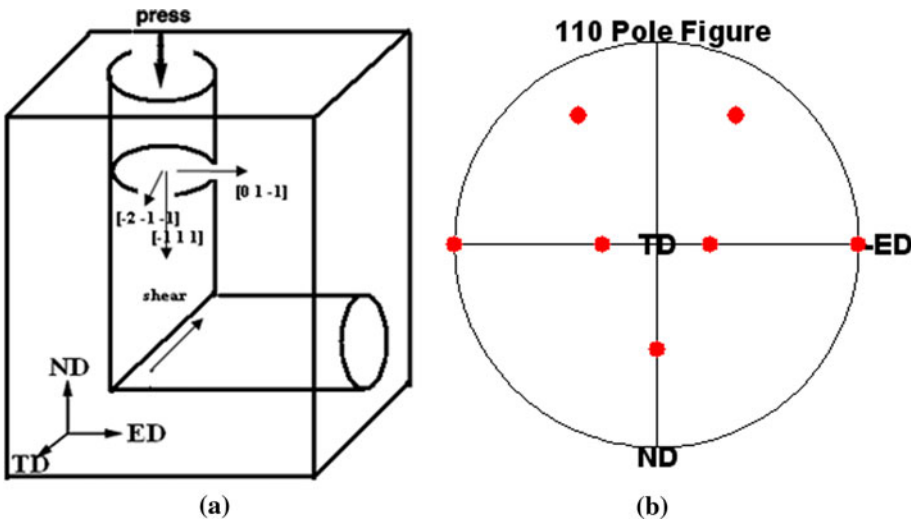

Fig. 1 The initial geometry and orientation of the single crystal

Experimental results

As it is expected that the macroscopic and microscopic grain splitting are related to the same underlying deformation mechanisms, it may be of benefit to perform scans on different length scales. Large scans over hundreds of microns have been conducted in the middle part of both cross-sections using SEM–EBSD with a step size of 2–3 μm. Mesoscopic scans with a smaller step size (about 0.3 μm) reveal more details of the interesting areas discovered inside the large scans. In addition, finer aspects of the substructures require even more detailed scans, usually with a step size of 50–100 nm.

Large scans

After ECAP deformation, the former single crystal exhibits pronounced straight misorientation bands that are about 350–450 μm regularly spaced and about 20–50 μm wide. In the transverse section they form an angle of about −22° with the transverse direction whereas in the longitudinal section an angle of about +28° with the extrusion direction (see Fig. 2a, c). These bands cross the whole sample and are slightly curved as they reach the edge of the sample. In the image quality (IQ) map, large misorientation bands are highlighted by a lighter color, indicating the existence of fewer dislocation structures inside the bands compared to the matrix. Based on the EBSD data, pole figures and misorientation angle plots are generated as shown in Fig. 3. The initial orientation is indicated by blue stars while the "orientation clouds" of the matrix after deformation are indicated by black dots and the large misorientation bands are red. The initial orientation is obviously focused on a small dot while the orientation after deformation is smeared out. The average orientation of the matrix changes only slightly, essentially by an anticlockwise rotation around TD. This is consistent with what is typically found in shear textures [13]. From the pole figures, there is no clear correlation between the large misorientation band and the initial orientation. However, the misorientation angle plots (Fig. 3b, d) show that the large misorientation bands have a constant disorientation (along the bands) of about 40°–50° with respect to the matrix in both sections. This is also confirmed by EBSD line scans through matrix and bands.

Mesoscopic scans

Figures 4 and 5 show details of the large misorientation bands on a mesoscale for both cross-sections. High angle

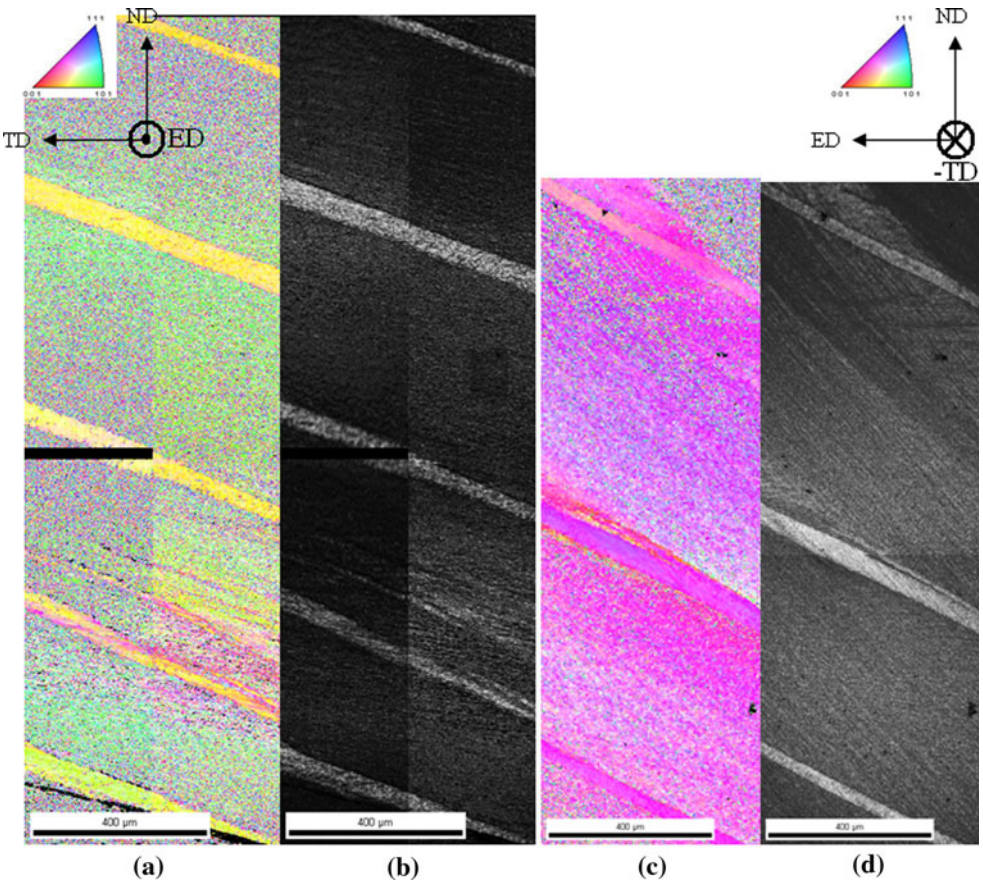

Fig. 2 EBSD scans on a large scale, **a** ED inverse pole figure in the transverse section, **c** TD inverse pole figure in the longitudinal section, and **b**, **d** the corresponding IQ maps

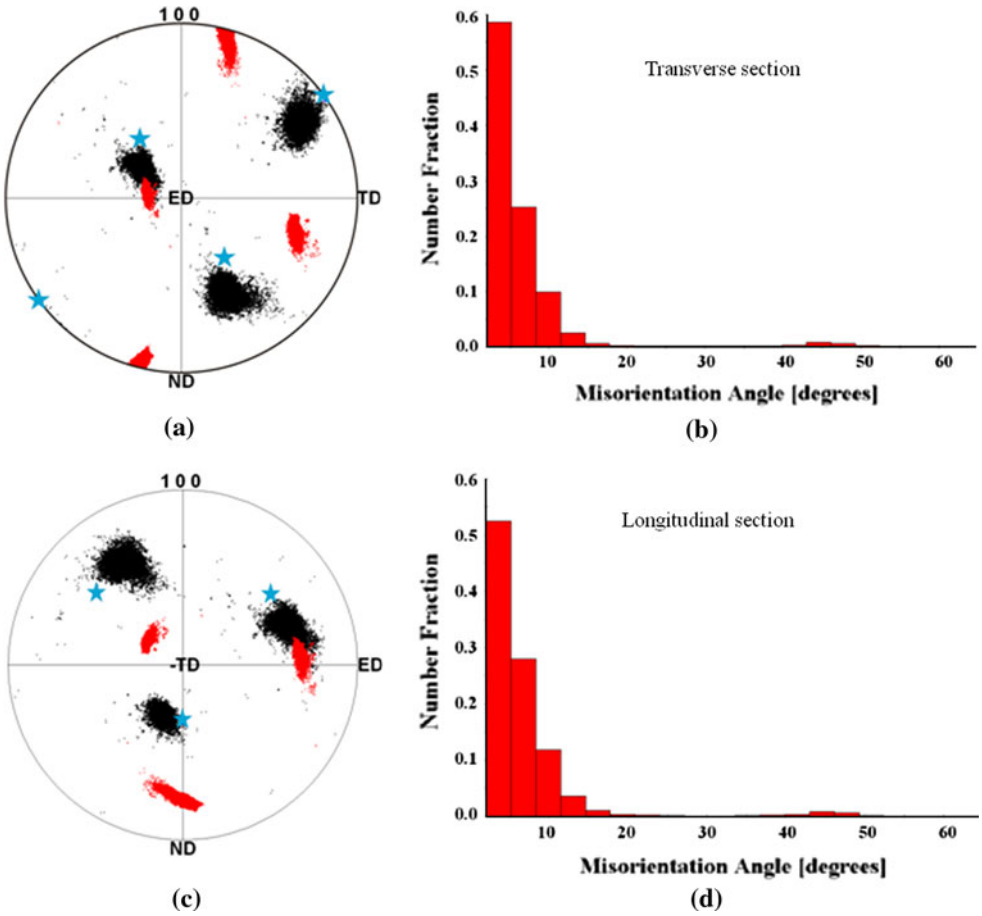

Fig. 3 100 pole figure of **a** the transverse section, **c** the longitudinal section, and the corresponding misorientation angle plots (**b**, **d**), *blue dots* in **a** indicates the initial crystal orientation, the *black dots* reveal the orientation of the matrix after deformation and the *red dots* the orientation of the large misorientation bands (Color figure online)

grain boundaries are indicated by black lines and low angle grain boundaries are marked in blue. The band shows less dislocation structures (rotation boundaries) than the matrix, which is confirmed by a lighter color in the corresponding IQ maps. The microstructure of the matrix in the transverse section displays only one set of microbands lying −19° to TD while in the longitudinal section two sets of microbands, one lying 45° to ED and another one parallel to ED. A group of discontinuous dislocation boundaries is observed in the misorientation bands, lying in the same direction as some of the dislocation structures in the matrix.

Detailed scans

The detailed scan (see Fig. 6) exhibits two intersecting sets of microbands. The intersections found in the horizontal bands indicate that at least the bands aligned with the simple shear plane are bands of localized shear or micro shear bands. The misorientation across the microbands is between 2° and 15°, which is roughly estimated by line scans normal to the microbands. Within this scan, the fraction of high angle grain boundaries indicated by thick black lines is close to 6%, excluding the influence of the large misorientation bands and the non-indexed points. It has been reported that the boundaries in heavily deformed metals do not only originate from grain boundaries present in the undeformed metal, but also originate from dislocation boundaries formed during grain subdivision. Qualitatively it has been proven that these boundaries have a large angular spread and that the misorientation across many boundaries is of the magnitude characteristic of ordinary high angle boundaries [14]. Therefore, only after one pass of ECAP deformation, high angle grain boundaries are generated by local shear deformation.

Based on these observations, a schematic 3D image of the microstructure in the single crystal was sketched as shown in Fig. 7. The large misorientation bands in both sections form a misorientation sheet and the single trace of the microbands in the transverse section is believed to correspond to the traces of two sets of microbands in the longitudinal section. The single crystal after deformation is split into regions by a group of evenly spaced misorientation sheets. In between these sheets, the matrix is subdivided by two sets of microbands.

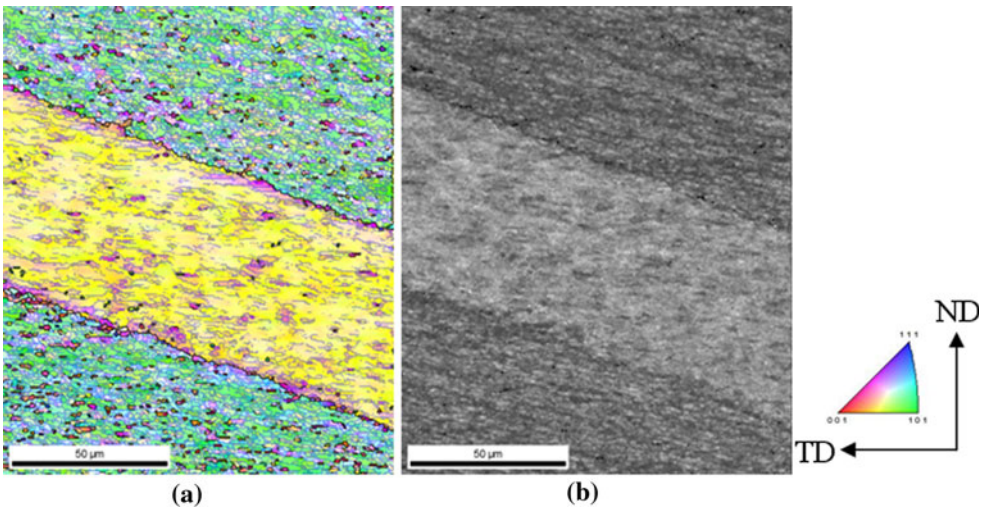

Fig. 4 **a** ED inverse pole figure on a mesoscale on the transverse section, **b** image quality map

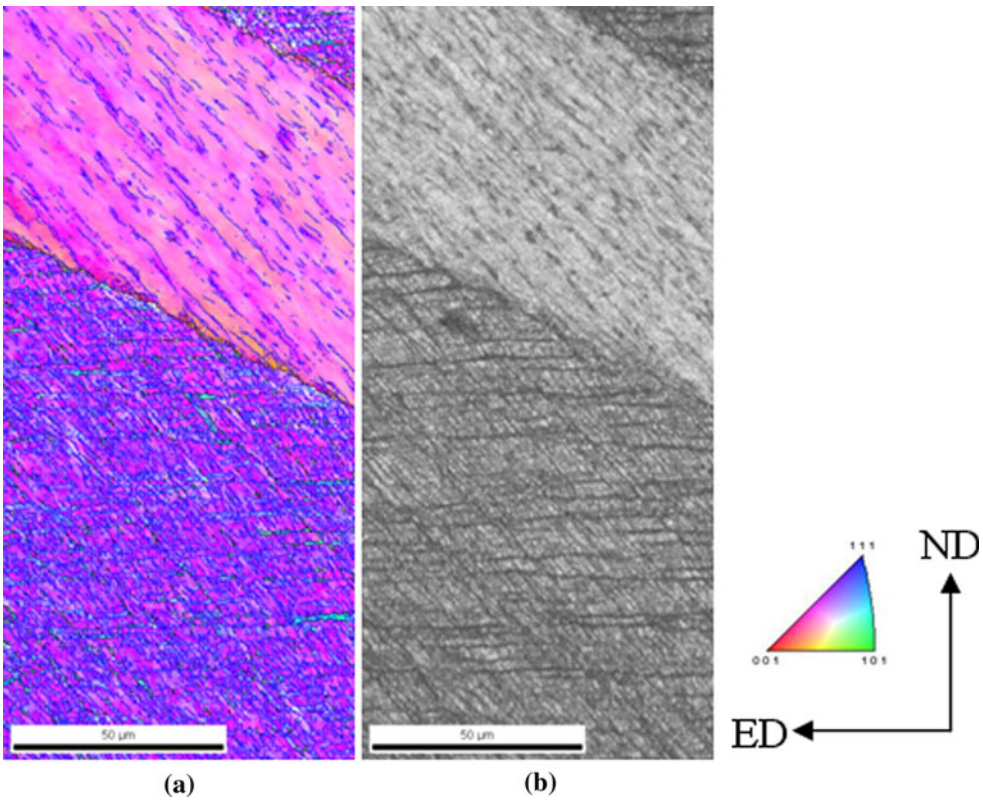

Fig. 5 **a** TD inverse pole figure on a mesoscale on the longitudinal section, **b** image quality map

Discussion

Data processing

The morphological orientation of the planar dislocation boundary is an important structural parameter that helps to relate the deformation at the grain scale to the one at the macroscopic scale. As sketched in Fig. 7, the matrix of the single crystal is subdivided by two sets of planar dislocation boundaries which form one group of boundary traces in the transverse section and two groups of boundary traces in the longitudinal section. The correlation between the morphological orientations of these two boundaries and the initial grain orientation is particularly interesting for this single crystal. In addition, the morphological orientation of the large misorientation sheets is also interesting.

Determination of the three-dimensional orientation of boundaries is usually based on transmission electron microscopy observations of the boundary traces, e.g., when the boundary orientation is close to a crystallographic plane

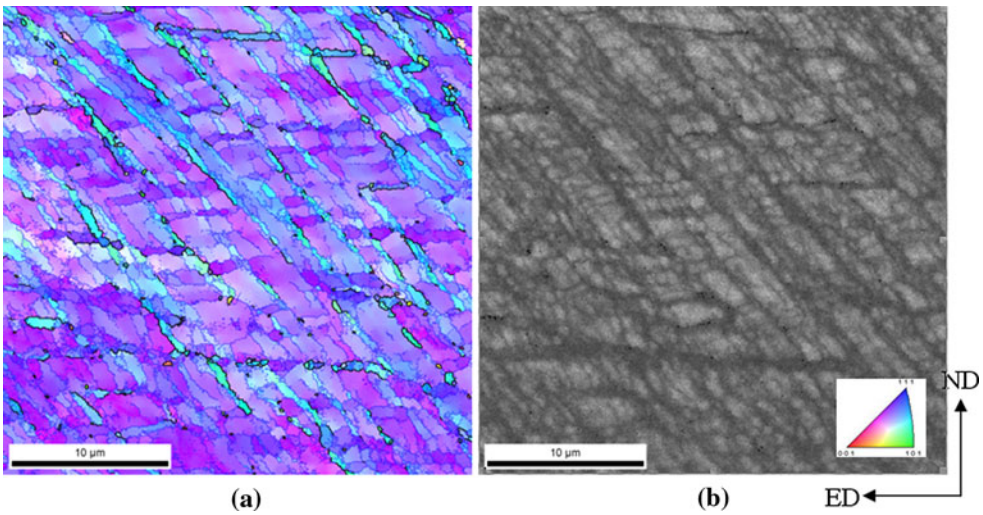

Fig. 6 **a** TD inverse pole figure of the matrix in the longitudinal section, **b** image quality map

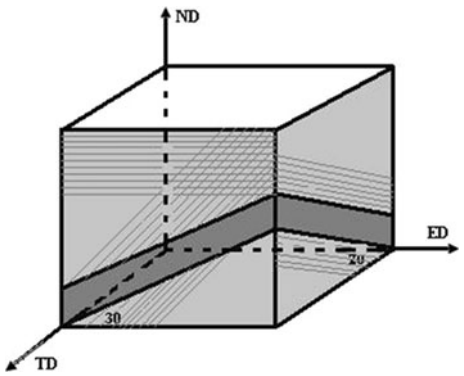

Fig. 7 Sketch of the microstructure in the single crystal after one pass ECAP deformation

of low index, the boundary orientation can be determined directly by tilting the sample until the boundary appears sharpest [15]. However, this technique is not easy to use and prone to human error. The 3D orientation analysis utilized in this work is based on a single observation of the boundary in the scanning microscope to obtain the angle between the boundary traces and the macroscopic deformation axes. Since the crystallographic directions parallel to the macroscopic axes are given by the EBSD scan, the alignment direction of the boundary trace can be calculated. Subsequent analysis of the boundary traces measured in different cross-sections of the single crystal allows the determination of the 3D boundary orientation by simply calculating the cross-product of the boundary traces.

Nevertheless, different EBSD scans could have different sample reference frames, especially for scans on different cross-sections. This means that the crystallographic orientations of the same microstructure observed in different scans are most likely represented by different but equivalent orientations. Thus, these representations are not comparable. A global sample reference frame needs to be established first and then all the measured EBSD data are processed according to the rotation matrix between the global and local sample reference frames.

Lattice rotation

The initial sample reference frame before ECAP deformation is chosen as global sample reference frame. Therefore, the orientations of the matrix with respect to the three macroscopic axes (ED, ND, and TD) before and after deformation are calculated and listed in Table 1. Decomposing the angle differences on three macroscopic axes leads to the amount of rotation around different axes. It gives that during ECAP deformation, the lattice rotated $+20°$ around TD, $-2°$ to $-3°$ around ND and $+2°$ to $3°$ around ED.

Slip geometry

For a single crystal deformed by a given deformation mode, it is possible to predict the slip systems activated at the beginning of the deformation. A volume conserving deformation can always be accommodated by a limited number of slip systems parallel to the planes and directions of highest resolved shear stress. Since the complete stress tensor for ECAP deformation is unknown yet, it is not possible to calculate the Schmid factors for potential slip systems. However, it is widely accepted that the deformation mode operating in ECAP deformation is simple shear on the intersecting plane of the inlet and outlet channels [13]. Therefore, instead of calculating the Schmid factor, we calculate the characteristic angles between the

Table 1 The angle difference between the lattice and the macroscopic axes before and after deformation

After	Before		
	TD ‖ [−2 −1 −1]	ED ‖ [0 1 −1]	ND ‖ [1 −1 −1]
TD ‖ [−0.80 −0.38 −0.46]	3.5°	86.8°	88.7°
ED ‖ [−0.17 0.88 −0.44]	92.3°	20.8°	110.7°
ND ‖ [0.58 −0.27 −0.77]	92.8°	69.3°	20.9°

Table 2 Angles between the potential slip planes and the simple shear plane

Slip plane	Angle to the SSP
(0 1 1)	55°
(0 1 −1)	45°
(1 0 −1)	77°
(1 0 1)	69°
(1 −1 0)	21°
(1 1 0)	69°

possible slip planes and the simple shear plane, and then consider the activated slip system as the one with the smallest characteristic angle, i.e., the closer to the simple shear plane, the easier to be activated.

TEM observation on commercially pure Nb deformed at room temperature indicated the activation of only {1 1 0} ⟨1 −1 1⟩ slip systems [16]. Therefore, only 12 slip systems are taken into account in this study. Among them, the (1 −1 0) plane is the macroscopically most stressed plane and is believed to be activated during deformation (see Table 2).

Characteristics of the large misorientation sheets

As observed in Fig. 2 and sketched in Fig. 7, the single crystal is separated by a group of evenly distributed sheet structures. The traces of this large misorientation sheet are 22° to TD and −28° to ED. On the other hand, the initial slip geometry (Fig. 8) shows that the most active potential slip plane (1 −1 0) forms traces close to these ones both in the transverse section and the longitudinal section. The deviation is smaller than 3°. Therefore, the large misorientation sheet actually matches very well with the initial position of the most active potential slip plane. Although the misorientation sheet exhibits much less dislocation structure inside, the strong misorientation with respect to the surrounding matrix indicates that the deformation mode operating inside the band is far from simple shear along the band plane and thus from single slip in the most favorably oriented slip system.

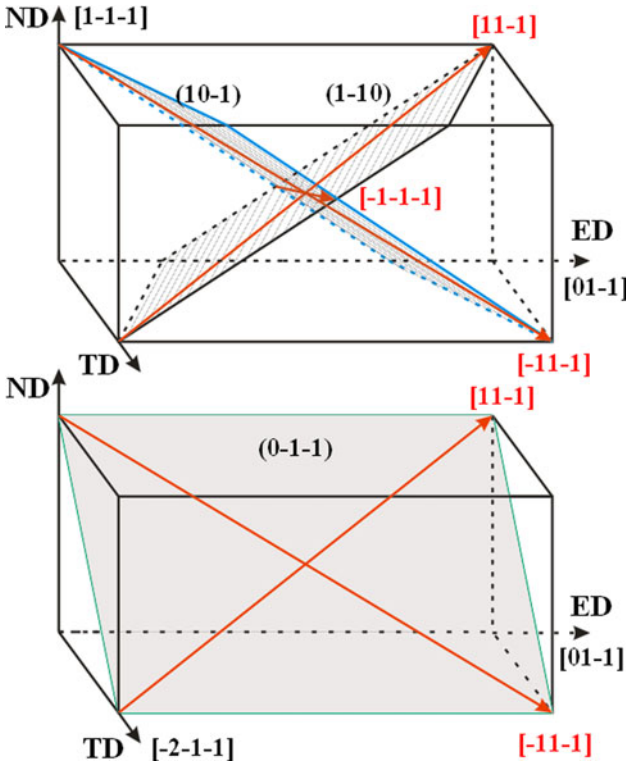

Fig. 8 Sketch of slip geometry in the single crystal before deformation

Dislocation boundary characteristics and slip system analysis

Whether the dislocation structures after deformation are macroscopically aligned to the most stressed plane or crystallographically aligned to the activated slip plane has been widely discussed. A large amount of experiments for different deformation modes has been conducted to support the existence of preferred macroscopic and crystallographic boundary planes [4, 6, 7].

In the present case, BCC Nb with high stacking fault energy was deformed by ECAP to a true strain of 1.15. As observed in the scans on the longitudinal section, one trace of straight dislocation boundaries is lying 45° to ED, which is located on the simple shear plane. However, the boundary trace in the transverse section is away from the

simple shear plane. Therefore, the boundary plane formed in the present work is not macroscopically aligned to the simple shear plane. Considering the +20° lattice rotation during deformation, however, it is found that one slip direction [1 1 −1] was actually rotating towards and finally very close to the simple shear plane. Early reports [17] have indicated that when the slip is concentrated on a few slip planes, the boundary plane lies close to the macroscopically most stressed planes. When the slip is distributed, no boundary plane is macroscopically aligned in most cases. Instead, the slip directions align with the macroscopically most stressed planes. This conclusion is based on FCC materials of medium to high stacking fault energy during deformation to low and moderate strains. For ECAP, the simple shear plane is believed to be the macroscopically most stressed plane. Therefore, our results show that for BCC Nb one slip direction aligns with the macroscopically most stressed plane after deformation as well.

The morphological orientations of the boundary plane are calculated from the EBSD data. For a single crystal, the boundary of the microband can be observed in both cross-sections. An analysis of the angles between the boundary trace and the macroscopic deformation axes leads to an exact orientation of the boundary trace. Subsequently, the morphological orientation of the boundary plane is calculated. In Fig. 7, boundary trace $\vec{a}$ is parallel to [0.31 0.45 −0.84] while boundary trace $\vec{b} \parallel$ [−0.17 0.88 −0.44], and $\vec{c} \parallel$ [−0.77 −0.43 −0.48]. It is believed that the two boundary planes observed in the longitudinal section have the same boundary trace $\vec{c}$ in the transverse section. Thus, the boundary plane with boundary traces $\vec{a}$ and $\vec{c}$ is (0.58 −0.79 −0.21) (1.2° deviated from (3 −4 −1)) while the one with $\vec{b}\vec{c}$ is (0.61 −0.26 −0.75) (5° from (2 −1 −3)). Both boundary planes are not simply aligned with a possible slip plane. An attempt has been made to roughly estimate the slip combinations which end up with this observed boundary planes.

Extensive experimental observations show that the dislocation structures are common to a range of metals, alloys, and deformation modes. The deformation-induced dislocation boundaries (GNBs and IDBs) subdivide the grain into small volume fragments. During plastic deformation, the misorientations across both GNBs and IDBs increase with increasing strain. The correlation between these boundaries and the active slip system is interesting. A recent article [7] reviews the slip system dependence of the dislocation structures for FCC materials, where the slip system configurations have been decomposed into fundamental slip classes and each slip class leads to a unique dislocation structure. The author [7] believes that the same slip class activated in different deformation mode, including shear deformation, leads to the same dislocation structure. In this study, we assume that BCC materials behave in the same way as FCC materials and attempt to find the correlation between the boundary planes and the {1 1 0} slip planes.

Among all the fundamental slip classes, both single slip and coplanar slip lead to boundaries closely aligned with the slip plane or slightly deviated to the slip plane. This deviation from the slip plane is reported to be smaller than 10° in most cases of FCC metals [7]. Therefore, the Miller index of the forming boundary plane resulting from single or coplanar slip would be very close to one of {1 1 0}. However, in our crystal the boundary planes are (3 −4 −1) and (2 −1 −3) as calculated above. This means that neither single slip nor coplanar slip could explain the microstructure. For collinear slip, the boundary plane always contains the common slip direction and its Miller index is the linear combination of the two collinear slip planes weighted by their respective slip activities (Schmid factor). For this single crystal, although the Schmid factor cannot be calculated, it is still clear that the Schmid factors for each possible slip system are different. The possibility exists, therefore, that the crystal was broken up by activating two groups of collinear slip systems and each combination ended up with one of the observed boundary planes. The first collinear slip operates on slip direction [1 1 −1] and forms the 45° aligned microbands while the second one glides on direction [−1 1 −1] and forms the horizontal microbands.

Simple shear simulated by the full constraints Taylor model

A full constraints Taylor simulation is applied to predict the orientation evolution during ECAP. The deformation mode is simple shear and the local sample reference frame is defined such that axis 1 parallel to shear direction, axis 3 parallel to TD. The applied velocity gradient tensor in this local sample reference frame is defined by a matrix

$$L = \begin{bmatrix} 0 & -\dot{\gamma} & 0 \\ 0 & 0 & 0 \\ 0 & 0 & 0 \end{bmatrix} \quad (2)$$

where $\dot{\gamma} = 2\cot\frac{\Phi}{2} = 2$. For details see [13].

Through matrix rotation, this velocity gradient tensor is expressed with respect to the global sample reference frame where a 10 steps FC-Taylor simulation is conducted. For consistency, slip systems {1 1 2} ⟨1 1 −1⟩ are artificially suppressed in the simulation by assigning them a large shear stress compared to those of slip systems {1 1 0} ⟨1 −1 1⟩.

The predicted orientation is 20.2° away from the matrix orientation found in reality and of course no large misorientation bands are predicted. The orientation evolution is

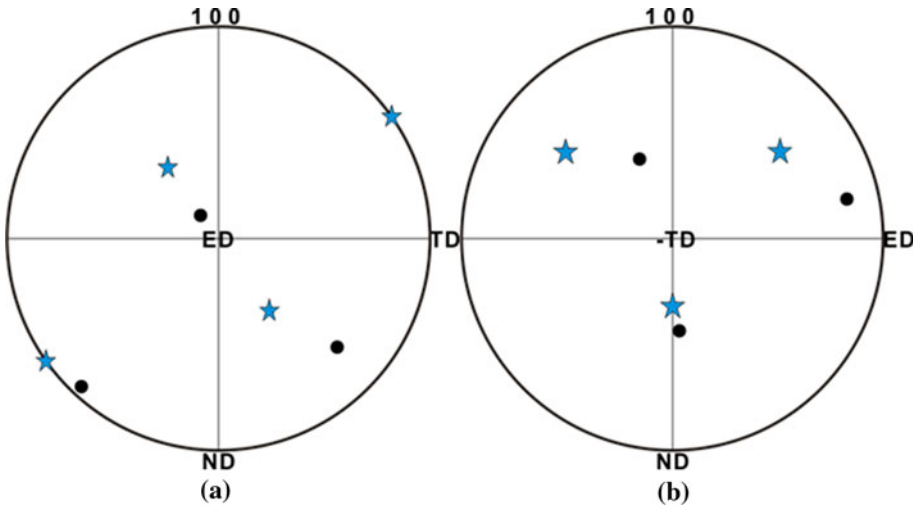

Fig. 9 100 pole figures of the orientation evolution simulated by FC-Taylor, the initial orientation is indicated by *blue stars* while the finial orientation is indicated by *black dots*, **a** in the transverse section, **b** in the longitudinal section (Color figure online)

plotted using pole figures both in the transverse section and in the longitudinal section as shown in Fig. 9. From both pole figures, an anticlockwise TD rotation is pronounced. This is in agreement with the experimental results (see Fig. 3). However, a large ND rotation (clockwise) is also observed. Checking the predicted active slip system step by step, it is found that the most active slip system is (1 −1 0) [1 1 −1] throughout the 10 steps simulation. The predicted active slip systems are not always the same for different modeling steps, but the main ones are sketched in Fig. 8, i.e., three slip planes, (1 −1 0), (1 0 −1), and (0 1 1), along directions [1 1 −1], [−1 1 −1], or [1 1 1]. Slip systems along [1 1 −1] always have a larger shear rate than slip systems along [−1 1 −1]. This shear amplitude difference results in a positive lattice rotation around TD and a negative rotation around ND. Although the slip systems activated along [1 1 1] give positive shear amplitudes around ND, these positive shear amplitudes are not large enough to cancel the negative shear amplitude. Therefore, a negative lattice rotation around ND is predicted by FC-Taylor in this case. However, this is not observed in experiments. The constraints of the die might prevent the lattice rotation around TD to a large extent, consequently, resulting in the 20° difference between the orientations predicted by FC-Taylor and the experimental results. Instead, a group of large misorientation sheets were formed to accommodate the redundant macroscopic deformation.

The Taylor model always gives a slip combination of minimum five slip systems in each simulation step. Most of those slip systems with high shear rates are all activated along the slip direction [1 1 −1] and [−1 1 −1]. As discussed above, we believe that slip systems along [1 1 −1] (collinear slip) form the microbands 45° to ED and the collinear slip along [−1 1 −1] form the horizontal microbands.

Comparison with some FCC single crystals

Several earlier reports [18–25] documented the processing of FCC single crystals by ECAP using initial orientations of 0° [18, 20], 20° [18, 19], and −20° [21]. In copper single crystals, one pass of ECAP leads to arrays of elongated cells having measured average widths of ∼0.2 μm. In aluminum single crystals, there were similar arrays of elongated microbands but the measured average width after a single pass was ∼1.3 μm. The higher values in Al are attributed to the high stacking fault energy and the high rate of recovery. In this work, the width of the microband is mainly between 0.8 and 1.2 μm. Since Nb has high stacking fault energy, this value is similar to the one of Al.

Different behaviors of lattice rotations were observed in ECAPed FCC metals. The lattice orientation remained the initial orientations or rotated for 20°, 40°, and even 60° around TD in a counter-clockwise sense. In this work, a counter-clockwise rotation of 20° around TD is also observed. In many cases, it is reported that the long axes of the microbands lie parallel to the slip traces of the primary {1 1 1} ⟨−1 1 0⟩ slip system [19, 20, 23]. However, in our case, the long axes of the microbands are not parallel to any {1 1 0} ⟨1 −1 1⟩ slip systems. Instead, they are parallel to the boundary plane formed by a collinear slip.

Conclusions

A niobium single crystal was subjected to ECAP at room temperature after orienting the crystal such that [1 −1 −1] ‖ ND, [0 1 −1] ‖ ED, and [−2 −1 −1] ‖ TD.

1. Macroscopically, the crystal is homogeneously subdivided by a group of evenly distributed misorientation

sheets. Microscopically, the crystal matrix exhibits a well formed cell structure with two sets of microbands. Instead of the microbands parallel to the simple shear plane, one slip direction is macroscopically aligned to the simple shear plane.

2. The matrix orientation changes mainly around the TD axis for 20° in a counter-clockwise sense. 6% of high angle grain boundaries in the matrix were generated by one pass of ECAP deformation.
3. The large misorientation sheets match very well with the most favorably oriented slip system and have a less pronounced substructure evolution than the matrix.
4. The full constraints Taylor model is used to simulate the slip activities during ECAP. The predicted results are partially similar to the experimental observations. Collinear slip systems are believed to be activated during the deformation.

Acknowledgements The authors gratefully acknowledge the financial support from the Belgian Science Foundation (FWO) under contact number G.0379.07 and the financial support from the Inter-university Attraction Poles Programme—Belgian State-Belgian Science Policy (Contract P6/24) as well as the helpful discussions with Anand Kanjarla and Steven Van Boxel. One of us, HRZS, acknowledges the support provided by Conselho Nacional de Desenvolvimento Científico e Tecnológico (CNPq, Brazil).

References

1. Liu Q, Hansen N (1998) Proc R Soc Lond A 454:2555
2. Godfrey A, Juul Jensen D, Hansen N (1998) Acta Mater 46:823
3. Godfrey A, Juul Jensen D, Hansen N (1998) Acta Mater 46:835
4. Winther G, Huang X, Hansen N (2000) Acta Mater 48:2187
5. Wert JA, Huang X, Inoko F (2003) Proc R Soc Lond A 459:85
6. Huang X, Winther G (2007) Phil Mag 87:5189
7. Winther G, Huang X (2007) Phil Mag 87:5215
8. Valiev RZ, Langdon TG (2006) Prog Mater Sci 51:881
9. Segal VM (1995) Mater Sci Eng A197:157
10. Fukuda Y, Oh-ishi K, Furukawa M, Horita Z, Langdon TG (2006) Mater Sci Eng A 420:79
11. Sandim HRZ, Bernardi HH, Verlinden B, Raabe D (2007) Mater Sci Eng A467:44
12. Iwahashi Y, Wang J, Horita Z, Nemoto M, Langdon TG (1996) Scr Mater 35:143
13. Beyerlein IJ, Toth LS (2009) Prog Mater Sci 54:427
14. Hughes DA, Hansen N (1997) Acta Mater 45:3871
15. Huang X (2005) Mater Sci Technol 21:1379
16. Seefeldt M, Zhu L, Wang B, Idrissi H, Schryvers D, Verlinden B (2009) In: Grivel JC, Hansen N, et al (eds) Proceedings of 30th Riso International Symposium on Materials Science, pp 309–316
17. Winther G (2003) Acta Mater 51:417
18. Fukuda Y, Oh-ishi K, Furukawa M, Horita Z, Langdon TG (2007) J Mater Sci 42:1501. doi:10.1007/s10853-006-0753-9
19. Fukuda Y, Oh-ishi K, Furukawa M, Horita Z, Langton TG (2006) Mater Sci Eng A 420:79
20. Fukuda Y, Oh-ishi K, Furukawa M, Horita Z, Langton TG (2004) Acta Mater 52:1387
21. Furukawa M, Kawasaki Y, Miyahara Y, Horita Z, Langdon TG (2005) Mater Sci Eng A 410–411:194
22. Miyamoto H, Erb U, Koyama T, Mimaki T, Vinogradov A, Hashimoto S (2004) Philos Mag Lett 84(4):234
23. Miyamoto H, Fushimi J, Mimaki T, Vinogradov A, Hashimoto S (2005) Mater Sci Eng A 405:221
24. Han WZ, Zhang ZF, Wu SD, Li SX (2007) Acta Mater 55:5889
25. Furukawa M, Horita Z, Langdon TG (2010) Mater Sci Forum 638–642:1946